Variation of half-life and internal-conversion electron energy spectrum between ^{235m}U oxide and fluoride

Y. Shigekawa,[1,*] Y. Kasamatsu,[1] Y. Yasuda,[1] M. Kaneko,[2] M. Watanabe,[2] and A. Shinohara[1]

[1]*Graduate School of Science, Osaka University, 1-1 Machikaneyama, Toyonaka, Osaka 560-0043, Japan*

[2]*Nuclear Science and Engineering Center, Japan Atomic Energy Agency, 2-4 Shirakata, Tokai-mura, Naka-gun, Ibaraki 319-1195, Japan*

(Received 18 April 2018; published 5 July 2018)

The nuclear half-life of ^{235m}U has been reported to vary depending on the chemical environment. In this study, both the half-life and the internal-conversion (IC) electron energy spectrum were measured for ^{235m}U with identical chemical environments for the first time. ^{235m}U oxide and fluoride samples were subjected to these measurements, and clear differences in the half-life and the energy spectrum between these samples were observed. The peaks in the energy spectra were identified with a relativistic density functional theory calculation. The molecular orbital states of the ^{235m}U oxide and fluoride, which were estimated from the energy spectra and the calculation, qualitatively explained the difference in the half-lives between the samples.

DOI: 10.1103/PhysRevC.98.014306

I. INTRODUCTION

It is widely known that the nuclear decay "constant" (half-life) is inherent in each nucleus and does not vary depending on the external environment, such as the pressure, temperature, or chemical environment. This is because the α, β, and γ decays are independent of the atomic electrons, and the electron-capture (EC) and the internal-conversion (IC) processes involve interactions with the inner-shell electrons, which are not usually affected by the external environment. However, only a few nuclides that decay by the EC and IC processes (e.g., ^{7}Be, ^{90m}Nb, ^{99m}Tc, and ^{235m}U) involve an interaction with the outer-shell electrons, and there are several reports that the half-lives of such nuclides vary depending on the chemical environments [1–5]. Recently, a large half-life variation of ^{229m}Th depending on the oxidation numbers was reported [6,7]. Studying the processes of the half-life variation is interesting and should help us understand the interaction between the wave functions of the nucleus and the atomic electrons.

The ^{235m}U isomer is an interesting nuclide in that its half-life varies considerably, on the order of several percent [4,5]. ^{235m}U ($I = 1/2^{+}$) is the first excitation state of ^{235}U ($I = 7/2^{-}$) and dominantly decays by the IC process in the $E3$ transition (IC coefficient $> 10^{10}$ [8]). Because the excitation energy above the ground state is only approximately 76.8 eV [9], the nucleus of ^{235m}U can interact only with the outer electron shells (i.e., $5f_{5/2}$, $5f_{7/2}$, $6s_{1/2}$, $6p_{1/2}$, $6p_{3/2}$, $6d_{3/2}$, $6d_{5/2}$, and $7s_{1/2}$). According to the measurement of the IC electron energy spectrum [9–11] and the theoretical calculation [12,13], $6p_{1/2}$ and $6p_{3/2}$ electrons are dominantly involved in the IC process. Indeed, the half-life of ^{235m}U has been reported to vary depending on the chemical environment; the half-life was increased by increasing the oxidation number of ^{235m}U in uranium oxides [4], and the decay constant clearly varied depending on the base metal into which ^{235m}U was implanted [5]. Although the half-life variation exhibited a certain tendency in these experiments, the mechanism underlying the variation is not well understood. Measurement of the IC electron energy spectrum should elucidate the half-life variation; however, the energy spectrum and the half-life have never been related to each other. In this study, for the first time, we determined the relationship between the half-life and the IC electron energy spectrum for the same chemical environment. Moreover, we compared the half-lives and the energy spectra between the ^{235m}U oxide and fluoride, and the half-life variation was qualitatively explained with the help of density functional theory (DFT) calculations.

II. EXPERIMENT

To measure the half-lives and the IC electron energy spectra of ^{235m}U, a retarding-field electron analyzer [14,15] was developed, as shown in Fig. 1. Three Ni electroformed meshes (transparency 88%) and a metal mesh (transparency 80%) were placed in parallel between the ^{235m}U sample and a two-stage microchannel plate (MCP) detector (HAMAMATSU F1942-04G, effective area of diameter 77 mm). By applying a negative retarding voltage to the intermediate two meshes, the energy of the electrons could be analyzed. The large solid angle between the sample and the MCP detector (1.2π sr) yielded a high total detection efficiency ($\sim$8%). The high efficiency was of great importance for analyzing the energy of the IC electrons of ^{235m}U because the half-life of ^{235m}U is short ($\sim$26 min) and the number of electrons that escape from the solid surface is low owing to the extremely small inelastic mean free path of low-energy electrons in solids [16]. The energy calibration of the analyzer was performed by measuring the Auger electrons from the ^{88}Zr electrodeposited source (77, 100, and 127 eV [17]).

^{235m}U samples were prepared using the Collection Apparatus for Recoil Products (CARP) [18]. ^{239}Pu, which decays

*shigekaway13@chem.sci.osaka-u.ac.jp

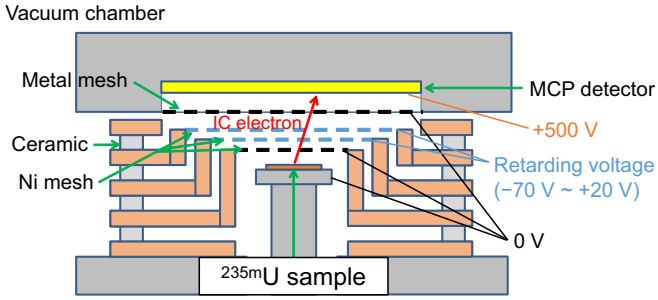

FIG. 1. A schematic view of the retarding-field electron analyzer for measuring the half-lives and the IC electron energy spectra of ^{235m}U.

to ^{235m}U (branching ratio = 99.9% [8]), was first purified [19–23] and electrodeposited on a Pt foil [24]. The thickness of the ^{239}Pu electrodeposited source (diameter 18 mm) was $10.5 \pm 0.2\ \mu g/cm^2$. In this study, three kinds of ^{235m}U samples were prepared. One was the ^{235m}U on the surface of the Cu sheet, which was obtained by collecting ^{235m}U recoiling out of the ^{239}Pu source to the Cu sheet with the CARP by setting the pressure of the apparatus as 1 atm of N_2 gas and applying −600 V to the Cu sheet. The others were ^{235m}U that reacted with the reactive gases: HF/N_2 mixture gas or pure O_2 gas, at 100 °C for 5 min after ^{235m}U was collected on the Cu sheet using the CARP. The prepared samples were put into the electron analyzer, and, after the pressure was below 1.3×10^{-4} Pa, the half-life measurement or the IC electron energy spectrum measurement was started. The MCP signals originating from the IC electrons were preamplified (device ORTEC VT120), amplified (REPIC RPN-092), and then discriminated (ORTEC 584) before being counted using a multichannel scaler (SEIKO EG&G MCA7000). In the half-life measurement, the retarding voltage was kept at 0 V, and the count was recorded with a dwell time of 30 s. In the measurement of the energy spectra, the retarding voltage was swept between −70 V and +20 V. The measurements of the half-life and the energy spectrum were repeated several times for each sample.

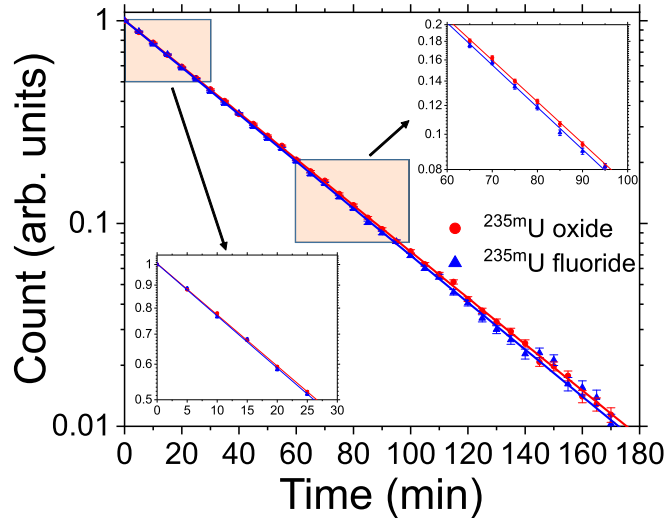

FIG. 2. Examples of the decay curves obtained for the ^{235m}U on the Cu sheet (red circle) and the ^{235m}U that reacted with HF/N_2 gas (blue triangle). The vertical axis indicates the IC electron counts during 5 min with arbitrary units. The error of each plot is the standard deviation of the counts. The insets show the decay curves for 0–30 min and 60–100 min with expanded scales.

TABLE I. Half-lives obtained for the ^{235m}U on the Cu sheet, ^{235m}U that reacted with the HF/N_2 gas, and the ^{235m}U that reacted with the O_2 gas. Each half-life was obtained by fitting the decay curve with a single exponential function after subtracting the constant background. The error of each half-life was determined by taking into account the standard deviations of the electron counts and the fitting. The half-lives measured for each sample were subjected to a weighted average. The gas reaction times for the HF/N_2 gas and the O_2 gas were 5 min except for the seventh run (7 min) and the eighth run (10 min) for the HF/N_2 gas. Note that the half-lives for the ^{235m}U that reacted with the HF/N_2 gas did not depend on the reaction time of the gas and thus the chemical reactions should reach equilibrium.

Sample	Run number	Half-life (min)
^{235m}U on the Cu sheet	1	26.40 ± 0.06
	2	26.39 ± 0.05
	3	26.38 ± 0.05
	4	26.30 ± 0.05
	Average	26.37 ± 0.03
^{235m}U that reacted with the HF/N_2 gas	1	25.91 ± 0.07
	2	26.01 ± 0.08
	3	25.81 ± 0.10
	4	25.87 ± 0.07
	5	26.10 ± 0.07
	6	25.96 ± 0.06
	7 (7 min)	26.10 ± 0.07
	8 (10 min)	25.92 ± 0.08
	Average	25.97 ± 0.03
^{235m}U that reacted with the O_2 gas	1	26.25 ± 0.09
	2	26.35 ± 0.08
	3	26.49 ± 0.09
	4	26.01 ± 0.10
	5	26.42 ± 0.08
	6	26.37 ± 0.07
	Average	26.33 ± 0.03

III. RESULTS

The results of the half-life measurement are shown in Table I. For the ^{235m}U on the Cu sheet, the half-lives obtained in four measurements agreed well within the standard deviation, and the half-life was determined to be 26.37 ± 0.03 min. In a previous study [4], the half-life for $^{235m}UO_3$ was determined to be approximately 26.1–26.6 min, which is close to the value obtained in our experiment. Therefore, it is considered that the ^{235m}U on the Cu is $^{235m}U^{VI}$ oxide. The half-life for the ^{235m}U that reacted with the O_2 gas was determined to be 26.33 ± 0.03 min, as shown in Table I. Having the same half-life for the ^{235m}U on the Cu sheet as for the ^{235m}U that reacted with the O_2 gas indicates that the ^{235m}U on the

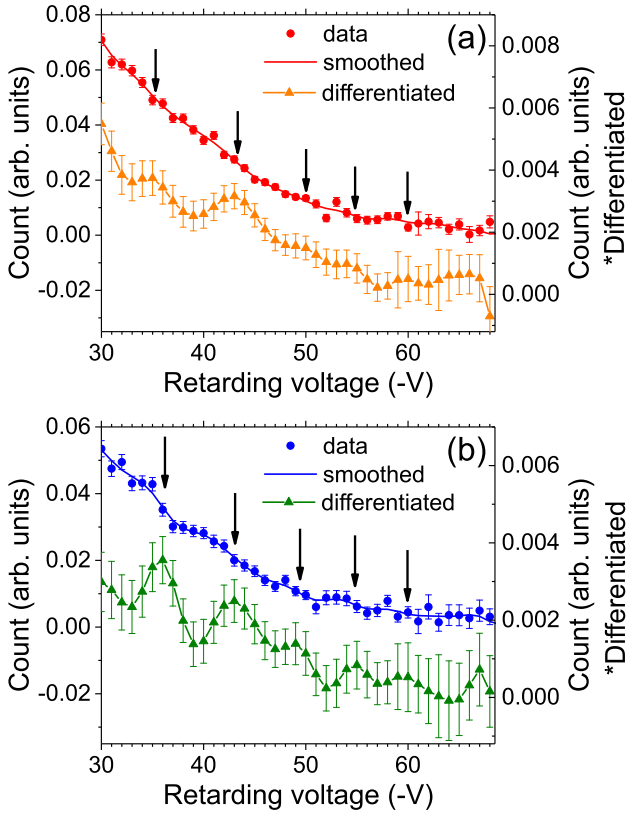

FIG. 3. The IC electron energy spectra obtained for (a) the ^{235m}U on the Cu sheet and (b) the ^{235m}U that reacted with HF/N_2 gas. The data obtained with several measurements were subjected to a weighted average. The averaged data (circle) were smoothed five times with five points (solid line) and then were differentiated with five points (triangle and solid line) with the Savitzky-Golay method [25]. The left vertical axes correspond to the counts of the averaged data and the smoothed data, and the right vertical axes correspond to the counts of the differentiated data. The arrows show the positions of the peaks in the differentiated data. The details of the peak positions and areas are described in Table II.

Cu sheet was quickly and fully oxidized to hexavalent uranium. On the other hand, as shown in Fig. 2, the slope of the decay curve for the ^{235m}U that reacted with the HF/N_2 gas clearly differs from that for the ^{235m}U on the Cu sheet. The half-life for the ^{235m}U that reacted with the HF/N_2 gas was determined to be 25.97 ± 0.03 min (see Table I), which is $1.506 \pm 0.002\%$ shorter than that for the ^{235m}U on the Cu sheet. This is the first determination of the half-life for ^{235m}U fluoride, and a clear difference in the half-lives between ^{235m}U oxide and fluoride was observed.

The IC electron energy spectra for the ^{235m}U on the Cu sheet and the ^{235m}U that reacted with HF/N_2 gas are shown in Figs. 3(a) and 3(b), respectively. The differentiated data represent the IC electron energy distribution emitted from the ^{235m}U samples. Five peaks were observed in each spectrum. The peak positions described with the binding energies of uranium and the areas are listed in Table II. Because the binding energies of the peaks A1, A2, A3, B1, B2, and B3 are close to the binding energies of the $6p_{1/2}$ and $6p_{3/2}$ electrons of the atomic uranium (26.8 and 16.8 eV, respectively [27]), the peaks are considered to correspond to the $6p$ electrons of uranium. The A4, A5, B4, and B5 peaks are considered to correspond to the $6d$ electrons, considering the result of the theoretical calculation [13]. In this study, only the $6p$ peaks (A1, A2, A3, B1, B2, and B3) are discussed, because the statistics for the $6d$ peaks (A4, A5, B4, and B5) are insufficient, and the contribution of the $6d$ electrons to the IC process should be 10 times smaller than that of the $6p$ electrons [13].

IV. CALCULATION

For a peak identification of the energy spectra, a relativistic DFT calculation was employed. The chemical forms of the ^{235m}U on the Cu sheet and the ^{235m}U that reacted with the HF/N_2 gas were assumed to be $[U^{VI}O_2(OH)_4]^{2-}$ (uranyl hydroxide) and $[U^{VI}O_2F_4]^{2-}$ (uranyl fluoride), respectively. The relativistic DFT calculations were performed via the

TABLE II. The peak positions and areas of the IC electron energy spectra in Figs. 3(a) and 3(b). The positions and areas of the peaks were obtained by fitting with the Gaussian function after subtracting the background originating from inelastic scattered electrons with Sickafus's method [26]. The peak positions described with the retarding voltage were calibrated to the electron kinetic energies with the energy calibration line [Kinetic energy(eV) = retarding voltage$(-V) \times (0.91 \pm 0.03) + (17 \pm 3)$]. This line was obtained by measuring Auger electrons from the ^{88}Zr source. The electron kinetic energies were converted to the uranium binding energy with the known excitation energy of ^{235m}U (76.8 ± 0.5 eV [9]). The $6p$ area ratios were calculated from the areas of the $6p$ peaks (A1, A2, A3, B1, B2, and B3).

Sample	Peak Name	Retarding voltage (−V)	Binding energy (eV)	Area (a.u.)	$6p$ area ratio (%)
^{235m}U on the Cu sheet	A1	35.2 ± 3.0	24 ± 3.8	2.2 ± 0.4	24 ± 4
	A2	43.2 ± 4.5	16.8 ± 4.1	5.8 ± 0.2	66 ± 4
	A3	49.9 ± 2.9	10.7 ± 3.9	0.9 ± 0.1	10 ± 1
	A4	54.3 ± 3.1	6.6 ± 4	1.8 ± 0.2	-
	A5	59.6 ± 1.9	1.9 ± 3.9	0.55 ± 0.03	-
^{235m}U that reacted with the HF/N_2 gas	B1	35.9 ± 3.5	23.4 ± 3.8	7.5 ± 0.2	45 ± 3
	B2	43.0 ± 4.2	17 ± 4	5.9 ± 0.6	36 ± 4
	B3	49.4 ± 3.1	11.2 ± 3.9	3.2 ± 0.6	19 ± 4
	B4	54.7 ± 2.5	6.3 ± 3.9	1.6 ± 0.2	-
	B5	59.8 ± 3.5	1.7 ± 4.1	1.9 ± 0.3	-

TABLE III. The calculated binding energies and the $6p$ IC probability ratios for $[U^{VI}O_2(OH)_4]^{2-}$ and $[U^{VI}O_2F_4]^{2-}$. $6p$ IC probability ratios were calculated from the PDOS for the $6p$ orbitals (Fig. 4) and the calculated IC rate per electron for an atom of ^{235m}U [13].

	Orbital name	Orbital	Binding energy (eV)	$6p$ IC probability ratio (%)
$[U^{VI}O_2(OH)_4]^{2-}$	A1′	$6p_{1/2}$	20.8	31.2
	A2′ (a)	$6p_{3/2}$	18.0	23.6
	A2′ (b)	$6p_{3/2}$	14.4	25.3
	A3′	$6p_{1/2}$	10.6	19.9
$[U^{VI}O_2F_4]^{2-}$	B1′	$6p_{1/2} + 6p_{3/2}$	21.0	40.2
	B2′	$6p_{3/2}$	15.5	40.2
	B3′	$6p_{1/2}$	10.4	19.6

ORCA version 3.0.0 program [28] using the scalar-relativistic second-order Douglas-Kroll-Hess Hamiltonian [29,30] with segmented all-electron relativistically contracted basis sets [31,32], in which the Breit-Pauli spin-orbit coupling method [33] was considered perturbatively. Resolution of the identity approximation [34,35] was applied to both pure- and hybrid-DFT calculations to reduce the computational cost of self-consistent field calculations, whose convergence threshold and grid resolution during the iterations were set to the same conditions used in previous studies [36,37]. The results of the calculations are shown in Fig. 4. The $6p_{1/2}$ orbital was found to interact with the axial oxygen atoms of uranyl ions ($O = U^{VI} = O$) and to largely split into bonding and antibonding orbitals. The $6p_{3/2}$ orbital was found to interact with the equatorial hydroxide and fluoride ions. The orbital that interacts with the hydroxide ion splits symmetrically, while that which interacts with the fluoride ion splits asymmetrically. The partial densities of states (PDOSs) for the $6p$ orbitals, which indicate the extent to which uranium $6p$ electrons occupy each hybrid orbital, are also shown in Fig. 4. Using the PDOSs for $6p$ electrons in Fig. 4 and the theoretical IC rates per electron (called the electronic factor w_e) for an atom of ^{235m}U ($w_e(6p_{1/2})/w_e(6p_{3/2}) = 2.3$ [13]), the IC probability ratios for $6p$ orbitals were calculated, as shown in Table III.

V. DISCUSSION

The binding energies and the $6p$ area ratios for the B1, B2, and B3 peaks in Table II are very close to those for B1′, B2′, and B3′ in Table III. Therefore, it is considered that the chemical form of the ^{235m}U that reacted with the HF/N_2 gas was $[U^{VI}O_2F_4]^{2-}$. Indeed, the Gibbs free energy for uranyl fluoride is significantly lower than that for uranyl hydroxide and uranium trioxide [38]; thus, uranyl fluoride was considered to be easily formed with the HF/N_2 gas. The binding energies and the $6p$ area ratios for the A1 and A3 peaks in Table II are similar to those for the A1′ and A3′ peaks in Table III; thus,

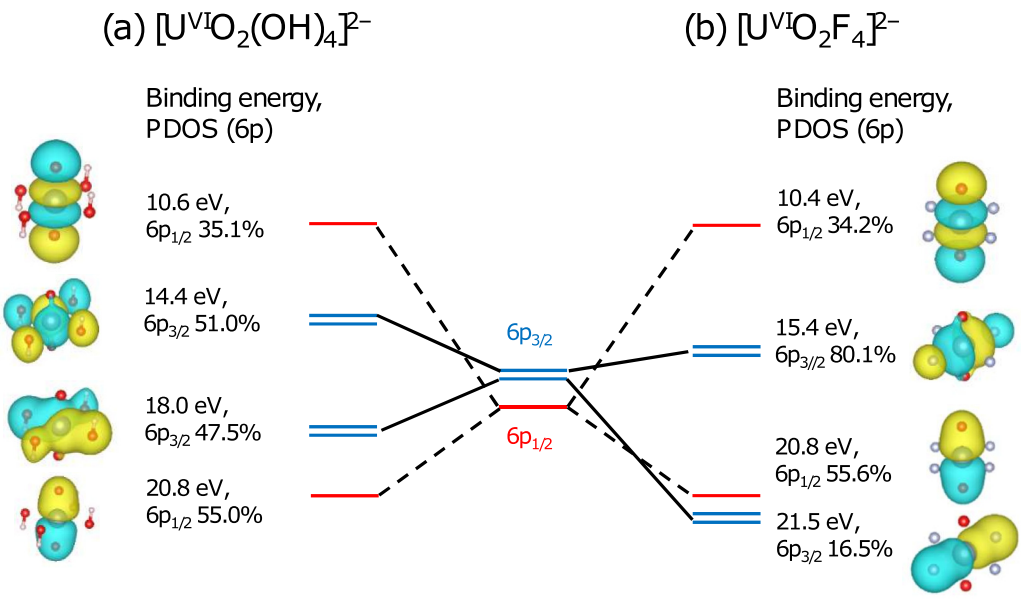

FIG. 4. The results of the DFT calculation at the B3LYP/TZVP//BP86/SVP level of theory for (a) $[U^{VI}O_2(OH)_4]^{2-}$ (uranyl hydroxide) and (b) $[U^{VI}O_2F_4]^{2-}$ (uranyl fluoride). In the molecular orbital diagram, $6p_{1/2}$ orbitals are described with the red single line, and $6p_{3/2}$ orbitals are described with the blue double lines. The binding energies and the partial densities of states (PDOSs) for $6p$ orbitals are shown next to the molecular orbital surface descriptions.

the $6p_{1/2}$ orbital for ^{235m}U on the Cu sheet interacts with the uranyl oxide. However, for the $6p_{3/2}$ orbital, only the A2 peak was observed, and peak splitting shown as A2′(a) and A2′(b) in Table III was not observed. This may be because not only uranyl hydroxide but also uranyl trioxide existed, making the peak broader than expected in the calculation. The interaction between the $6p_{3/2}$ orbital of the uranium atom and the $2s$ orbital of the oxide atom for uranyl trioxide is considered to be similar to that for uranyl hydroxide.

Finally, the origin of the half-life variation between the ^{235m}U oxide (^{235m}U on the Cu sheet) and the ^{235m}U fluoride (^{235m}U that reacted with the HF/N_2 gas) is considered on the basis of the measurement of the IC electron energy spectra and the DFT calculation. For $[U^{VI}O_2F_4]^{2-}$, 80% of the $6p_{3/2}$ electrons occupy the antibonding orbital, as shown in Fig. 4. This value is clearly larger than that of 51% for $[U^{VI}O_2(OH)_4]^{2-}$. The IC probability for the antibonding orbital is considered to be higher than that for the bonding orbital because the electron density around the ^{235m}U nucleus for the antibonding orbital is higher. Thus, the half-life for the ^{235m}U fluoride is shorter than that for the ^{235m}U oxide. The origin of the half-life variation between the ^{235m}U oxide and fluoride was explained according to the electron-orbital variation for the first time in this study.

VI. CONCLUSION

We observed that the half-life for the ^{235m}U fluoride is clearly shorter than that for the ^{235m}U oxide. Moreover, a clear difference in the IC electron energy spectra was observed, and the peaks were identified via relativistic DFT calculation. The origin of the shorter half-life for the ^{235m}U fluoride is considered to be the higher occupancy of the antibonding orbital by the $6p_{3/2}$ electrons, which provides a new insight into the deexcitation process of ^{235m}U.

ACKNOWLEDGMENTS

We are grateful to T. Munakata and T. Yamada—of the Graduate School of Science, Osaka University—for advice and support in the development of the retarding-field electron analyzer. This work was supported by JSPS KAKENHI Grant No. JP25800150.

[1] G. T. Emery, Ann. Rev. Nucl. Sci. **22**, 165 (1972).
[2] T. Ohtsuki, H. Yuki, M. Muto, J. Kasagi, and K. Ohno, Phys. Rev. Lett. **93**, 112501 (2004).
[3] H. Mazaki, S. Kakiuchi, T. Mukoyama, and M. Matsui, Phys. Rev. C **21**, 344 (1980).
[4] M. Neve de Mevergnies and P. Del Marmol, Phys. Lett. B **49**, 428 (1974).
[5] M. Neve de Mevergnies, Phys. Rev. Lett. **29**, 1188 (1972).
[6] L. v. d. Wense, B. Seiferle, M. Laatiaoui, J. B. Neumayr, H. J. Maier, H. F. Wirth, C. Mokry, J. Runke, K. Eberhardt, C. E. Düllmann, N. G. Trautmann, and P. G. Thirolf, Nature (London) **533**, 47 (2016).
[7] B. Seiferle, L. von der Wense, and P. G. Thirolf, Phys. Rev. Lett. **118**, 042501 (2017).
[8] E. Browne and J. K. Tuli, Nucl. Data Sheets **122**, 205 (2014).
[9] V. I. Zhudov, A. G. Zelenkov, V. M. Kulakov, V. I. Mostovoi, and B. V. Odinov, JETP Lett. **30**, 516 (1979).
[10] D. P. Grechukhin, V. I. Zhudov, A. G. Zelenkov, V. M. Kulakov, B. V. Odinov, A. A. Soldatov, and Yu. A. Teterin, JETP Lett. **31**, 592 (1980).
[11] A. D. Panov, JETP **85**, 313 (1997).
[12] D. P. Grechukhin and A. A. Soldatov, Yad. Fiz. **23**, 273 (1976) [Sov. J. Nucl. Phys. **23**, 143 (1976)].
[13] A. M. Frolov, Radiat. Phys. Chem. **72**, 541 (2005).
[14] N. J. Taylor, Rev. Sci. Instrum. **40**, 792 (1969).
[15] P. W. Palmberg, Appl. Phys. Lett. **13**, 183 (1968).
[16] M. P. Seah and W. A. Dench, Surf. Interface Anal. **1**, 2 (1979).
[17] L. E. Davis, N. C. MacDonald, P. W. Palmberg, G. E. Riach, and R. E. Weber, *Handbook of Auger Electron Spectroscopy*, 2nd ed. (Physical Electronics Industries, Edina, MN, 1976).
[18] Y. Shigekawa, Y. Kasamatsu, and A. Shinohara, Rev. Sci. Instrum. **87**, 053508 (2016).
[19] Y. Muramatsu, S. Uchida, K. Tagami, S. Yoshida, and T. Fujikawa, J. Anal. At. Spectrom. **14**, 859 (1999).
[20] R. F. Anderson and A. P. Fleer, Anal. Chem. **54**, 1142 (1982).
[21] J. Zheng, M. Yamada, Z. Wang, T. Aono, and M. Kusakabe, Anal. Bioanal. Chem. **379**, 532 (2004).
[22] T. C. Kenna, J. Anal. At. Spectrom. **17**, 1471 (2002).
[23] E. Chamizoa, M. C. Jimenez-Ramos, L. Wacker, I. Vioque, A. Calleja, M. Garcia-Leona, and R. Garcia-Tenorio, Anal. Chim. Acta **606**, 239 (2008).
[24] N. Trautmann and H. Folger, Nucl. Instrum. Methods A **282**, 102 (1989).
[25] A. Savitzky and M. J. E. Golay, Anal. Chem. **36**, 1627 (1964).
[26] E. N. Sickafus, Phys. Rev. B **16**, 1448 (1977).
[27] J. G. Fuggle and N. Martensson, J. Electron Spectrosc. Relat. Phenom. **21**, 275 (1980).
[28] F. Neese, WIREs Comput. Mol. Sci. **2**, 73 (2012).
[29] M. Douglas and N. M. Kroll, Ann. Phys. (N.Y.) **82**, 89 (1974).
[30] B. A. Hess, Phys. Rev. A **33**, 3742 (1986).
[31] D. A. Pantazis, X. Chen, C. R. Landis, and F. Neese, J. Chem. Theory Comput. **4**, 908 (2008).
[32] D. A. Pantazis and F. Neese, J. Chem. Theory Comput. **7**, 677 (2011).
[33] M. Reiher and A. Wolf, *Relativistic Quantum Chemistry - The Fundamental Theory of Molecular Science* (Wiley-VCH, Weinheim, 2009), Chap. 13, pp. 494–498.
[34] F. Neese, J. Comput. Chem. **24**, 1740 (2003).
[35] F. Neese, F. Wennmohs, A. Hansen, and U. Becker, Chem. Phys. **356**, 98 (2009).
[36] M. Kaneko, M. Watanabe, and T. Matsumura, Dalton Trans. **45**, 17530 (2016).
[37] M. Kaneko, S. Miyashita, and S. Nakashima, Inorg. Chem. **54**, 7103 (2015).
[38] D. D. Wagman, W. H. Evans, V. B. Parker, R. H. Schumm, I. Halow, S. M. Bailey, K. L Churney, and R. L. Nuttall, J. Phys. Chem. Ref. Data **11**, Suppl. 2 (1982).